Volume 1 | Number 1 | Jan 2013 | Pages 1–100

CrystEngComm

www.rsc.org/crystengcomm

ROYAL SOCIETY OF CHEMISTRY

ROYAL SOCIETY OF CHEMISTRY

www.rsc.org/crystengcomm

For table of contents use only
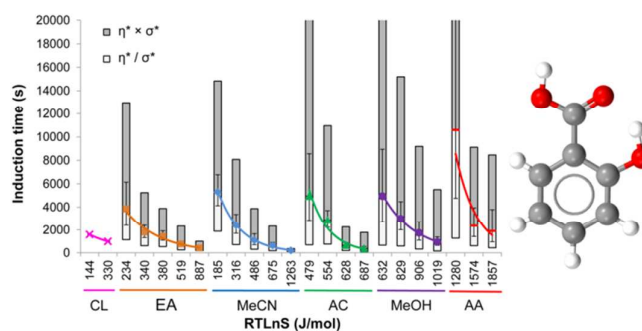
Nucleation of salicylic acid in different solvents becomes gradually more difficult in the order: chloroform, ethyl acetate, acetonitrile, acetone, methanol and acetic acid. By comparing the results of metastable zone width and induction time experiments new insights are obtained.

Crystal nucleation of salicylic acid in organic solvents

Donal Mealey[a], Denise M. Croker[a,*], and Åke C. Rasmuson[a, b].

[a] Synthesis and Solid-State Pharmaceutical Centre, Materials and Surface Science Institute, Department of Chemical and Environmental Science, University of Limerick, Ireland.

[b] Department of Chemical Engineering and Technology, KTH Royal Institute of Technology, Teknikringen 42, SE-10044 Stockholm, Sweden.

*Corresponding author: denise.croker@ul.ie

ABSTRACT

The crystal nucleation of salicyclic acid was explored in a range of solvents using induction time and metastable zone width measurements. In total 3100 experiments were performed to collect statistically valid nucleation results. The lognormal cumulative probability function provided a representative fit for both induction time and metastable zone width distributions. At equal driving force the induction time is found to increase in the order chloroform, ethyl acetate, acetonitrile, acetone, methanol and acetic acid, and this order agrees with the order of increasing interfacial energy The metastable zone width (MSZW) value (expressed as supersaturation driving force) was highest in acetic acid followed by a lower value in methanol, consistent with the induction time results. In ethyl acetate, acetonitrile and acetone the corresponding MSZW values were lower but the order among these three solvents varied depending on the cooling rate and saturation temperature. A novel format for comparing the induction time and MSZW experiments is presented. The analysis reveals that the time of nucleation in the metastable zone width experiments is also dependent on the time of transforming clusters into nuclei, and not only governed by the rate of supersaturation generation. The relative influence of this transformation time depends on the solvent and the cooling rate.

INTRODUCTION

Crystallization from solution is a unit operation of significant importance in the industrial manufacturing of inorganic and organic chemicals, with crystallization processes widely employed in the purification of pharmaceutical compounds. Mechanistically, crystallization processes are primarily governed by crystal nucleation and crystal growth. Both mechanisms are insufficiently understood, and process development is largely based on applied experiments on the particular compound of interest. Crystal nucleation is the first step in the formation of a solid phase in solution and does significantly influence product properties like crystal structure, particle size, purity, and yield. In order to form a nucleus of crystalline material that is thermodynamically stable at the prevailing conditions, the free energy barrier, arising as a result of the competition between the favorable crystal bulk free energy and the unfavorable solid-liquid interfacial energy, needs to be surpassed. However, the kinetic mechanisms involved are not well understood. In the classical theory of nucleation,[1-6] individual molecules continually attach to and detach from crystalline subcritical clusters. In the recently proposed two-step theory[7, 8], nucleation proceeds first by the emergence of droplet-like clusters of higher solute concentration, followed by an ordering within this cluster into a crystalline structure. Both theories are critiqued in a recent review article by Davey et al.[9]

The mechanisms of crystal nucleation of small molecules are difficult to investigate because the nucleation (i) occurs in the nanometer size range and within fractions of a second, (ii) has a very strong non-linear dependence on the driving force, and (iii) occurs in a solution that is thermodynamically unstable. A further complicating factor is that nucleation has a strong stochastic component, generally resulting in a large spread in nucleation data carried out under identical conditions.[10-17] This stochastic behavior can be regarded as an inherent feature of primary nucleation, or originating from e.g. a stochastic distribution of impurities[18], and tends to disappear at larger scales due to the impact of secondary nucleation [19]. Assuming that the nucleation is a perfectly random process the cumulative induction time distribution should be an exponential function.[15, 18, 20, 21].

Experimentally, two techniques are used to characterize nucleation behavior, both relying on the observation of the macroscopic outcome of the nucleation process. Induction time experiments (IDT) measure the time lapse between the initiation of supersaturation and the occurrence of nucleation at constant conditions. The experimentally observable induction time includes the time for pre-nucleation cluster formation in solution, the nucleation time, and the time to grow to detectable size, but normally the nucleation time is assumed to be governing[38]. Metastable zone width (MSZW) experiments determine the range of supersaturation where primary nucleation is

unlikely to occur within a practical time frame, and is determined in dynamic conditions usually involving a constant cooling rate. The metastable zone width is experimentally more easily determined than the induction time. The metastable zone width is often reported as the difference between the saturation and nucleation temperatures ($\Delta T = T_{sat} - T_{nuc}$) even though the corresponding supersaturation driving force would be a scientifically more useful parameter. Investigations reveal that the width of the metastable zone is influenced by agitation[39], additives[40], and rate of supersaturation generation[27, 41]. Both techniques were used concurrently by Kulkari et al. to investigate nucleation kinetics of isonicotinamide in ethanol, with the authors deducing that although MSZW measurements are easier to conduct, IDT measurements may be more accurate [44]. Sullivan et al. employed IDT measurements in a study to investigate molecular self-assembly and solution in the nucleation process [45].

In the present study, salicylic acid, first reported by Cochran in 1953[23], is used as a model compound, due to its single polymorphic form and availability of solubility data in a number of solvents of varying type[24-26]. The dominating feature of the crystal structure is the centrosymmetric carboxylic acid dimer (Figure 1). This dimer serves to provide great rigidity to the salicylic acid molecule which has been suggested to partly explain the lack of polymorphism and solid phase solvation. Nucleation data for salicylic acid in different solvents is presented, acquired from repeated induction time and metastable zone width type experiments. A comparison of induction time data and metastable zone width data is conducted and a format for this comparison is proposed which can help to further advance the understanding of crystal nucleation. In the analysis of the results, reference is made to the classical nucleation theory andthe two-step model, for the purpose of discussing kinetic and thermodynamic aspects of the nucleation process, however without the aim of establishing if either of these theories is governing this particular case.
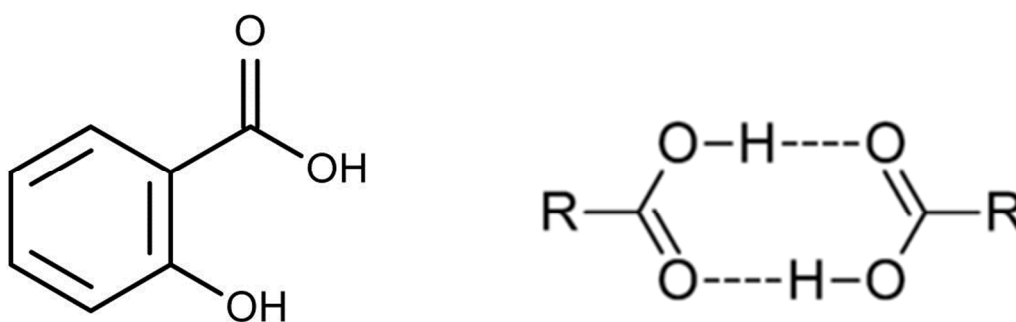
Figure 1: a) chemical structure of salicylcic acid and b) the carboxylic acid:acid dimer favoured in the crystal structure

EXPERIMENTAL

The model compound, salicylic acid, was purchased from Sigma-Aldrich (99.0%) and used without further purification. The solvents: Acetone (AC) (99.8%), Acetic acid (AA) (Glacial) (99.7%), Methanol (MeOH) (99.8%), Acetonitrile (MeCN) (99.8%), Chloroform (CL) (99.8%), and Ethyl acetate (EA) (99.8%) were all purchased from VWR International and used as received.

A saturated stock solution of salicylic acid in the pure solvent was prepared from published solubility data[24], at 250 mL scale in a sealed conical flask. Agitation was provided with a PTFE coated magnetic stirrer and solutions were allowed to equilibrate overnight, 5 °C above the saturation temperature. Twenty glass vials (70 x 25 mm, VWR International) were filled with 20 mL of the stock solution via preheated syringes and 0.2 μm filters (Millipore). For some experiments all vials contained the same solution; for other experiments ten vials were used for one solution and ten for another. A magnetic stir bar (13 x 3 mm, Type A, or 12 x 3 mm with 4 mm pivot ring, Type B; Figure 2) was added to each vial prior to sealing with a plastic screw cap and PTFE seal. The sealed vials were then left 5 °C above the saturation temperature overnight with agitation.

Induction time experiments

The induction time of salicylic acid was determined in six different solvents using a saturation temperature of 50 °C (with the exception of chloroform where the saturation temperature was 40 °C). Over 1100 induction time measurements were made across all six solvents at different nucleation temperatures. The experimental set-up used could operate and observe up to 20 individual nucleation experiments simultaneously. Two isothermal water baths (Grant S26 with GR150 control units and C2G cooling units) equipped with submersible multipole magnetic stirrer plates were employed, and the complete set of vials was moved from one bath to the other to achieve the step change in temperature required for the induction time experiments. In all experiments an agitation rate of 200 rpm was used. One bath (bath A) was maintained 5 °C above the saturation temperature (T_{sat}) of the solution being examined, and the second (bath B) was maintained at a set temperature (T_{nuc}) in the supersaturated region for the solution. Crystallization was detected using a high definition camcorder (Sony HDRXR520VE/Sony HDRXR350VE). Once nucleation occurred, the solution became completely milky within 1-2 seconds, except for in chloroform where it was within ~5 seconds. For each vial, the induction time is reported as the total time from introducing the tubes into the nucleation temperature water bath, to the time of the first detection of a change in the solution properties as recorded by the video camera and later examined by the naked eye. A reference vial (solvent only) with an in-

situ temperature probe (P600 Dostmann) was used to monitor the attainment of T_{nuc} in the vials after immersion into water bath B. The temperature decay follows an exponential curve and reaches T_{nuc} + 1 °C within 240 seconds, +0.5 °C within 275 seconds, and + 0.1 °C within 400 seconds.

For acetonitrile and ethyl acetate five different nucleation temperatures were investigated, for acetone and methanol four, for acetic acid three and for chloroform two. From previously published solubility data[22], the RTlnS value (S = C/C*; C = concentration in solution (g/g solvent), C* = solubility at T_{nuc} (g/g solvent) of each experiment was calculated as is given in Table 1. Approximately 50 induction time measurements at each nucleation temperature were made in each of ethyl acetate, acetonitrile, acetone and methanol. In acetic acid, 30 experiments and in chloroform 10 were made at each condition. The volatility of chloroform caused problems in sample preparation and due to the low solubility the nucleation detection limit is reduced. In acetic acid solutions the difficulty in triggering the nucleation of salicylic acid, even at high driving force, was evident with small sample numbers.

Metastable zone width determination

Metastable zone width measurements were performed in methanol, ethyl acetate, acetonitrile, and acetone to provide data for comparison with the induction time experiments. Solutions were saturated at 50 °C and cooled at 5, 10 or 15°C/hr until nucleation was observed, with agitation provided by a Type A stir bar. Additional experiments on the influence of the saturation temperature were conducted by cooling solutions saturated at 50, 40, and 30 °C at 10 °C/hr with agitation provided Type B stir bar.

The metastable zone width experiments were carried out in the same vials and using the same camcorders as in the induction time determinations. An external temperature probe (PT100) in the GR150 bath was used in conjunction with the control unit to set a linear cooling profile and to log temperature values versus time for analysis. The temperature at which each nucleation event occurred was measured and used to calculate the corresponding thermodynamic driving force. When the cooling cycle was completed and nucleation events detected, the sample tubes were heated up to the dissolving temperature again. Once all the salicylic acid had re-entered the solution phase, as observed visually, the tubes were allowed to equilibrate for a minimum of 4 hours before the cooling cycle was repeated. The cycle was repeated until at least 50 nucleation events had been recorded for a given set of conditions.

5

RESULTS AND EVALUATION

Induction times

Figure 2 presents a representative sample of the experimentally recorded induction time distributions obtained for salicylic acid in acetonitrile as a function of driving force. The use of the arithmetic mean and standard deviation to represent these distributions would be inappropriate due to the deviation from the normal distribution. Furthermore, depending on the thermodynamic driving force and solvent, in some instances some vials didn't nucleate within the total experimental time.
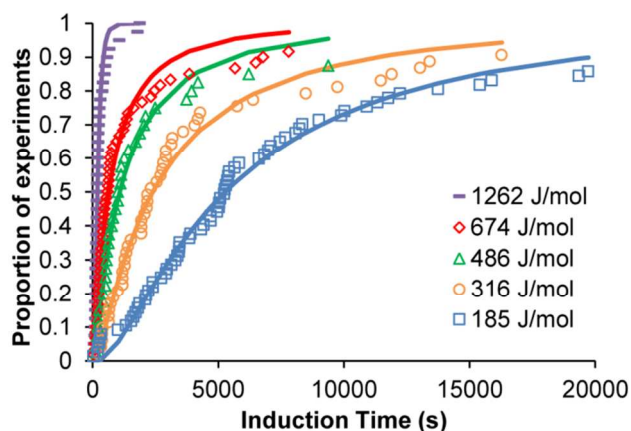
Figure 2. Induction time distributions of salicylic acid in acetonitrile (mole fraction = 0.059, saturated at 50°C) at various thermodynamic driving forces for nucleation (RTlnS). Also shown are fits of the lognormal distribution function to the data sets.

To account for vials not nucleated, to determine an adequate average value representing the distribution and to examine the shape of the induction time distributions, a variety of different distribution functions (Eq 1- 5) were fitted to the data by a least squares method. The fitting was performed such that those tubes which had not nucleated at all were accounted for in determining the proportion of tubes nucleated. The lognormal cumulative distribution function (LCDF) (Eq. 1) was found to provide the overall best fit, producing a coefficient of determination (CD) greater than 0.97 in all cases. Previous induction time nucleation studies[55,16], have used exponential based functions: Eq. 2 and 3, respectively. Eq 3 was found to produce fits giving a CD of 0.76, while the equation used by Diao et al.[22, 52], generated CD of 0.94. Other standard distribution functions were also examined such as the Weibull (Eq. 4) and the log-logistic functions (Eq. 5). Even though all these functions did provide reasonably adequate representations of the data, they were inferior to the lognormal function.

6

$$F(x) = \frac{1}{2} erfc \left[-\frac{\ln(x) - \eta}{\sigma\sqrt{2}} \right] \tag{1}$$

$$F(x) = e^{-x/\tau^\beta} \tag{2}$$

$$F(x) = 1 - e^{(-J V x)} \tag{3}$$

$$F(x) = 1 - e^{\left(- \left(\frac{x}{\lambda}\right)^\beta\right)} \tag{4}$$

$$F(x) = \frac{1}{1 + (\lambda/x)^\beta} \tag{5}$$

In fitting the LCDF, a location (η) and a scale parameter (σ) is determined that can be easily back-transformed to the geometric mean (η^*) and geometric standard deviation (σ^*) of the induction time distribution[42]. The geometric mean formally equals the median value (τ_{50}) of the induction time distribution, and in previous work has been found to provide an average representation of the induction time distribution that is less sensitive to experimental uncertainties[54]. The use of the geometric standard deviation as opposed to the traditional standard deviation allows for the interpretation of the asymmetry in the distribution of the data. All induction time distributions are summarized in Figure 3 and in Table 1. As is expected, in each case the geometric mean induction time decreases with increasing driving force, and for each solvent the distribution standard deviation decreases as the driving force increases, as shown in Figure 3.
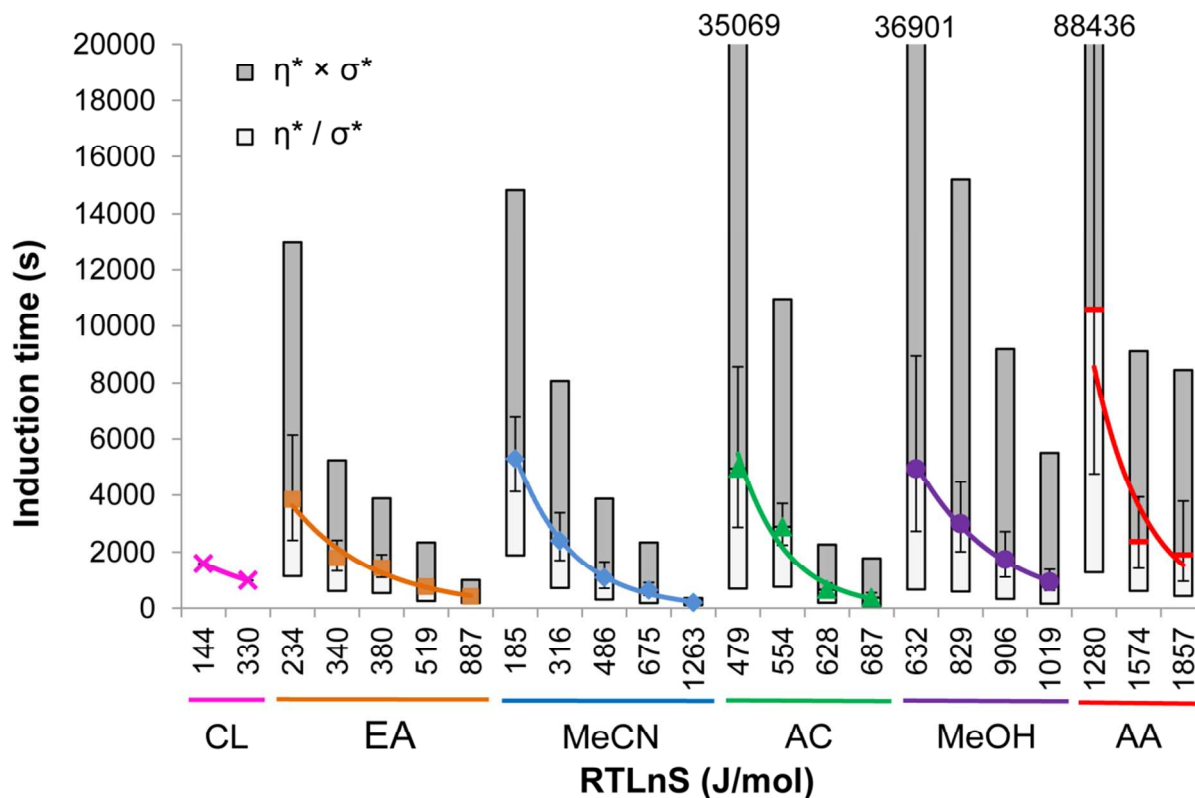
Figure 3. The effect of thermodynamic driving force (RTlnS) on the induction time distributions in; Chloroform (**x**), Ethyl Acetate (**■**), Acetonitrile (**♦**), Acetone (**▲**), Methanol (**●**), and Acetic acid (**━**). Symbols represent the geometric mean (η^*) position. The bars represent the 95% confidence interval for the geometric mean. The shaded regions represent 68% of the data ($\eta^* \times\!/ \sigma^*$). The ratio of the size of the upper shaded region to the lower is representative of the skew to the data. Where present, numbers above a data set indicate the uppermost value for that data set, included for necessity of scale.

8

Table 1. Induction time experiment results: The geometric mean (η^*), geometric standard deviation (σ^*), calculated nucleation rate (J), and size of the critical nucleus are shown. Also included for comparison is the calculated nucleation rate (J^a) obtained by the method of Jiang and ter Horst[16].

Solvent	S	T (°C)	RTlnS (J/mol)	η^* (s) $^\times\!/\sigma^*$	J ($m^{-3} s^{-1}$)	Critical nucleus Radius (Å)	Number of Molecules in Critical Nucleus	J^a ($m^{-3}s^{-1}$)
Chloroform	1.06	39	144	1587[b]	32	9.2	21	21[c]
	1.14	37	330	985[b]	51	4.0	2	43[c]
Ethyl Acetate	1.09	43.8	234	3844 $^\times\!/$ 3.37	13	14.5	82	9
	1.14	40.9	340	1784 $^\times\!/$ 2.94	28	9.9	27	19
	1.16	39.8	380	1438 $^\times\!/$ 2.70	35	8.9	19	23
	1.22	35.9	519	768 $^\times\!/$ 3.04	65	6.5	8	43
	1.43	25	887	416 $^\times\!/$ 2.39	120	3.8	2	81
Acetonitrile	1.07	47.6	185	5284 $^\times\!/$ 2.81	10	19.3	196	6
	1.13	45.8	316	2399 $^\times\!/$ 3.36	21	11.3	40	14
	1.20	43.5	486	1081 $^\times\!/$ 3.58	46	7.4	11	31
	1.30	40.9	675	640 $^\times\!/$ 3.65	78	5.3	4	52
	1.60	32.5	1263	199 $^\times\!/$ 1.82	251	2.8	1	165
Acetone	1.21	35	479	4947 $^\times\!/$ 7.09	10	14.8	88	7
	1.24	32.5	554	2883 $^\times\!/$ 3.80	17	12.8	57	11
	1.28	30	628	653 $^\times\!/$ 3.47	77	11.3	39	49
	1.32	28	687	368 $^\times\!/$ 4.82	136	10.3	30	77
Methanol	1.28	35	632	4937 $^\times\!/$ 7.47	10	12.3	49	6
	1.39	30	829	2994 $^\times\!/$ 5.08	17	9.3	22	10
	1.44	28	906	1730 $^\times\!/$ 5.31	29	8.5	17	19
	1.51	25	1019	933 $^\times\!/$ 5.90	54	7.6	12	33
Acetic acid	1.66	30	1280	10594 $^\times\!/$ 8.35	5	8.0	14	2
	1.89	25	1574	2363 $^\times\!/$ 3.86	21	6.5	8	14
	2.14	20	1857	1901 $^\times\!/$ 4.44	26	5.5	5	17

[b]median induction times [c]fitting function to small sample numbers n≈10

9

The shortest nucleation induction time was observed in chloroform. A driving force of 144 J/mol resulted in a median induction time of about 1,600 seconds and increasing the driving force to about 330 J/mol reduced the induction time to 985 seconds. For calculation of approximate nucleation parameters the median induction times obtained from the experiments have been used. The longest induction times were observed in acetic acid. At a driving force of 1,280 J/mol, only 68% of the samples had nucleated after 88,000 seconds. Besides chloroform, the mean induction times are reasonably short in ethyl acetate and acetonitrile. Nucleation occurred in a large proportion of the experiments at about RTlnS = 200 J/mol in less than 15000 seconds, while in acetone and methanol it took at least 3 to 4 times the driving force to reach similar induction times. To reach the same induction time in the different solvents the required driving force increases in the order: chloroform, ethyl acetate, acetonitrile, acetone, methanol and acetic acid.

Due to the non-parametric nature of the distributions the coefficient of variation needs to be examined while in the logarithmic scale where the distribution is normally distributed:

$$CV = \frac{\sigma}{\eta} \qquad\qquad [6]$$

As seen in Figure 4, there is a general trend towards higher coefficients of variation in moving from ethyl acetate (shortest induction time) to acetic acid (longest induction time) as a function of supersaturation driving force. However, in methanol the CV appears to be overall the highest. The spread in non-parametric data can also be examined by the coefficient of quartile variation[43], which shows roughly the same behavior, Figure 4.
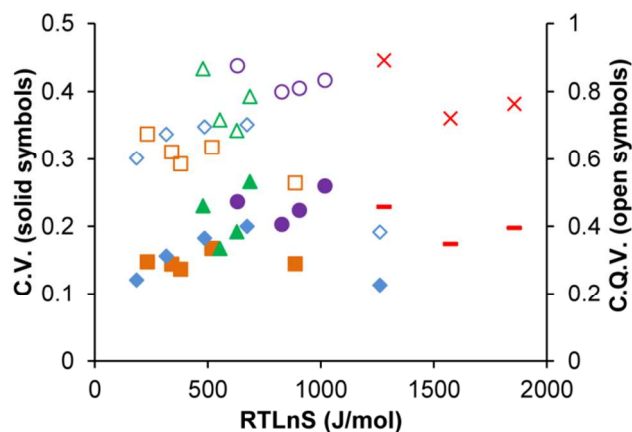
Figure 4. Coefficient of variation (CV) (solid symbols) and coefficient of quartile variation (CQV) (open symbols) for distributions of induction time experiments. Ethyl acetate (■), acetonitrile (♦), acetone (▲), methanol (●), and acetic acid (**X** (CV), ▬ (CQV)).

Figure 5 presents the standard evaluation plot according to the classical nucleation theory[16, 29, 40]. By relating the induction time (t_{ind}) to the nucleation rate (J) it is possible to estimate the pre-exponential factor (A) and the interfacial energy (φ) using equations 7 and 8:

$$\frac{1}{t_{ind}V} = J = A \exp\left(\frac{-\Delta G_{crit}}{R\,T}\right) \tag{7}$$

$$\Delta G_{crit} = \frac{16\pi N_A \varphi^3 \upsilon^2}{3(RT\ln S)^2} \tag{8}$$

where N_A is the Avogadro number, R is the gas constant, T is temperature, ΔG_{crit} is the nucleation work assuming a spherical nucleus, V is the volume of the solution, υ is the molar volume of salicylic acid in the cluster, and RTlnS is the supersaturation driving force. All data points for a particular solvent do not fall on a straight line, but there is a tendency for some curvature at increasing x-coordinate value, possibly indicating a mechanism transition[46]. Accordingly, the straight line fitting is based on the shorter induction time points as shown in the figure.
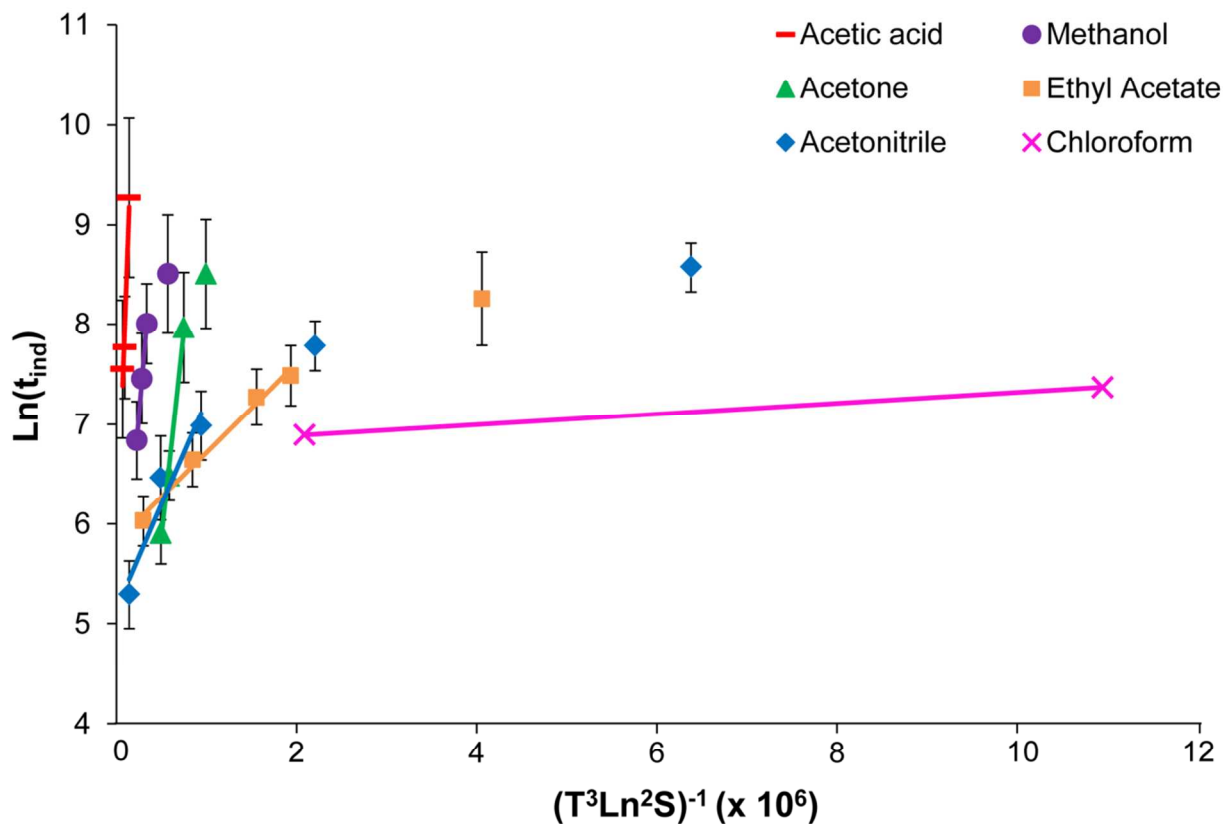
Figure 5. Evaluation of the induction time experiments according to the classical nucleation theory. Bars represent the 95% confidence interval for the geometric mean induction time from the lognormal distribution fit.

As shown in Table 2, the highest interfacial energy is found in acetic acid, followed in decreasing order by: methanol, acetone, acetonitrile, and ethyl acetate, with by far the lowest interfacial energy in chloroform. The pre-exponential factors are calculated from the intercept of the linear fits in Figure 6 by using equation 7 and are given in Table 2. The determination of the preexponential factors tends to be more uncertain than the determination of the interfacial energies, and especially when the graphs in figure 5 are very steep, e.g. for acetone. Nordström et al[51] proposed that the preexponential factor should be proportional to the solute concentration, C, times the square root of the solvent molecular weight, M, and divided by the solution dynamic viscosity, λ, here approximated by the solvent viscosity:

$$A \propto F_A = \frac{C\sqrt{M}}{\lambda} \qquad\qquad [9]$$

In chloroform, F_A, receives a low value because of the quite low solubility, and in methanol and acetone the F_A-value is high because of the high solubility. The correlation between the experimentally determined preexponential factors and the group F_A as estimated at relevant nucleation temperatures from equation 9 is shown in Figure 6. In acetone $F_A=104*10^3$ receives the highest value and the preexponential factor is clearly the highest: over 8000, however the point is not shown since it is clearly out of scale. As shown, F_A actually captures the order between the solvents in terms of preexponential factor with ethyl acetate being the only exception.
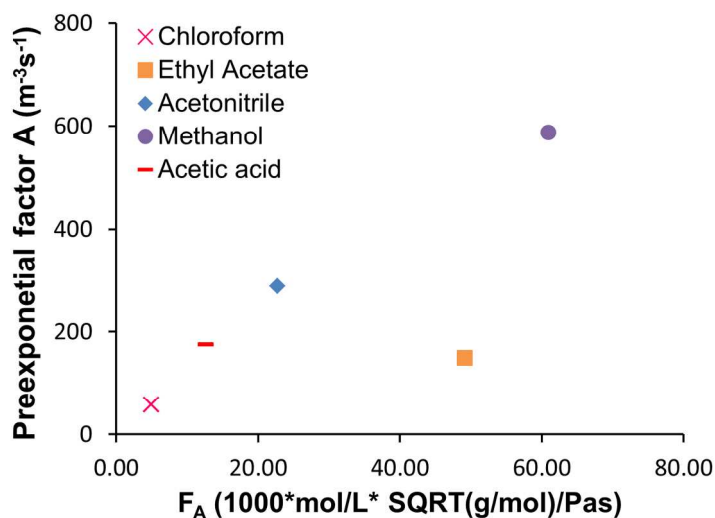
Figure 6. Correlation between the experimentally determined preexponential factors and F_A as per +-Equation 9. Acetone is omitted for necessity of scale (A = 8645 m^{-3}s^{-1})

The critical nucleus size, r_c, is calculated from the interfacial energy:

$$r_c = \frac{2v\varphi}{RTlnS}$$ [10]

and from that the corresponding number of molecules in the nuclei using the molecular volume of 9.572E-05 m^3/mol, Table 1. In a few cases the critical nucleus contains just one or two molecules. Even though a very low number of molecules in the critical nucleus has been reported before[47-49], this does not appear to be realistic since in our experiments we always on average have an induction time much larger than zero. The nucleation rate in Table 1 is calculated as the

inverse of the geometric mean induction time and the solution volume, eq 7. If the nucleation rate is calculated by the method of Jiang and ter Horst[16], the trends in the results appear to be the same but the absolute values are on average 30-50 % lower.

The nucleation work is plotted in Figure 7as calculated by Eq. 8, illustrating how the magnitude (J/mol) of the nucleation free energy barrier varies over the experimental range in each solvent. In acetic acid the interfacial energy is the highest, but the experiments are performed at much higher driving force leading to moderate nucleation work. However, the induction time tends to be longer in acetic acid as the pre-exponential factor is fairly low. In acetone and methanol, the interfacial energies are lower but the experiments are performed at lower driving forces leading to higher nucleation work. However this is balanced by higher pre-exponential factors leading to shorter induction times. The induction time ranges of methanol and acetone are fairly similar; in spite of that, the nucleation work tends to be higher in acetone. This reflects the much higher pre-exponential factor for acetone. In acetonitrile and ethyl acetate the interfacial energies are further lower but so are also the driving force ranges. In comparing the acetic acid data at RTlnS=1280 J/mol with the data for acetonitrile at RTlnS = 1263 J/mol the induction time is clearly longer in acetic acid because there is a substantial difference in the nucleation work. If we compare the acetic acid data at RTlnS=1857 with the data for acetonitrile at RTlnS=486 the nucleation work is fairly similar (Figure 7), but the induction time is shorter in acetonitrile because of the higher preexponential factor. Finally in chloroform the nucleation work is low (comparable to the lowest nucleation work calculated in ethyl acetate and acetonitrile), but achieved at a clearly lower driving force. The preexponential factor is clearly the lowest by which the induction times are still appreciable.

Table 2. Calculated interfacial energies and kinetic factors for salicylic acid nucleation in the different solvents.

Ease of nucleation (1-5)	Solvent	Interfacial energy[a] (mJ/m^2)	Pre-exponential factor[a], $A(m^{-3} s^{-1})$	Solubility at 25 °C [38]	
				(M.F.)	(Mol/l)
1	Chloroform	0.71	57	0.010^b	0.131^b
2	Ethyl Acetate	1.82	148	0.136	1.599
3	Acetonitrile	2.40	289	0.029	0.581
4	Acetone	3.81	8645	0.179	2.974
5	Methanol	4.13	586	0.128	3.628
6	Acetic acid	5.50	175	0.055	1.015

[a] Eq. 1, using lognormal distribution fits. [b] This work.
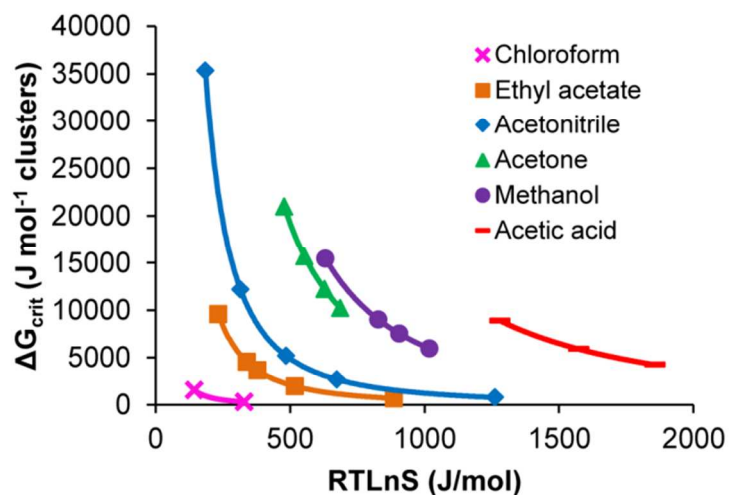
Figure 7. The nucleation work for salicylic acid in the different solvents over each respective experimental range as calculated from the interfacial energies of Table 2 by eq. 8 and experimental RTlnS values.

From the direct assessment of the experimental results (Figure 3), as well as from the interfacial energies determined in accordance with the classical nucleation theory, it is concluded that the nucleation gradually becomes more difficult, (i.e. the induction time at equal driving force gradually increases) in the order: chloroform, ethyl acetate, acetonitrile, acetone, methanol and acetic acid. The influence of the solvent on the nucleation rate does not clearly correlate with the solubility [53,29], the Hansen solubility parameter[54], or the solvent boiling point or enthalpy of vaporization[55]. As is shown in Table 3, it is noteworthy that even though eq 2 – 5 do not provide the optimum fit to experimental induction time distribution data, the interfacial energies do not change much with the function used, and the order between the solvents doesn't change at all.

Table 3. Calculated interfacial energies from using different statistical functions to represent induction time distributions.

Solvent	Interfacial energy (mJ/m^2)					
	Lognormal	Median	Weibull	Log-log	Jiang [15]	Diao [20]
Chloroform	-	0.71	-	-	-	-
Ethyl acetate	1.82	1.79	1.81	1.82	1.72	1.83
Acetonitrile	2.40	2.34	2.42	2.40	2.24	2.52
Acetone	3.81	3.77	3.79	3.81	3.73	3.75
Methanol	4.13	3.81	4.11	4.13	4.03	4.05
Acetic acid	5.50	5.45	5.53	5.52	5.49	5.70

Metastable zone widths

The metastable zone width distributions contain the randomness of the nucleation process as well as the effect of the constantly changing driving force, and are more "S-shaped" than the induction time distributions. Representative examples of distributions are shown in Figure 8. In general the highest supersaturation driving forces at nucleation are recorded in methanol, followed by acetonitrile, acetone and ethyl acetate, at this cooling rate. The lognormal cumulative distribution function (LCDF) was found to also accurately represent the metastable zone width driving force (RTlnS) distributions at all cooling rates and concentrations, creating coefficients of determination greater than 0.97. The results are given in Table 4 and 5 below as the geometric mean RTlnS values (η^*) with geometric standard deviations (σ^*) and the undercooling (ΔT) corresponding to the geometric mean RTlnS.
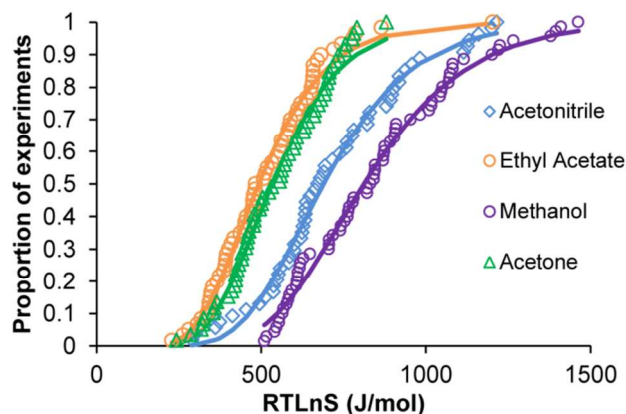
Figure 8. Metastable zone width distributions in different solvents. Saturation temperature: 50°C. Cooling rate: 15 °C/hr. Agitation provided by stirring bar type A at 200 rpm. Also shown are fits of the LCDF to the data.

17

Table 4. Metastable zone width determinations at different cooling rates in solutions saturated at 50 °C Geometric mean driving forces (η*), geometric standard deviations (σ*), and corresponding undercooling (ΔT). Stir bar: type A.

Cooling rate:	5°C/hr			10°C/hr			15°C/hr		
Solvent	ΔT	η*	σ*	ΔT	η*	σ*	ΔT	η*	σ*
Ethyl acetate	11.12	400	1.443	13.43	482	1.385	13.72	493	1.389
Acetonitrile	5.62	394	1.531	7.15	506	1.464	9.68	689	1.363
Acetone	13.22	403	1.391	16.13	491	1.357	17.52	533	1.359
Methanol	12.34	514	1.366	17.48	720	1.301	19.73	812	1.358

Table 5. Metastable zone width determinations at different saturation temperatures at cooling rate of 10 °C/hr. Geometric mean driving forces (η*), geometric standard deviations (σ*), and corresponding undercooling (ΔT). Stir bar with pivot ring: type B.

Saturation temperature:	30°C			40°C			50°C		
Solvent	ΔT	η*	σ*	ΔT	η*	σ*	ΔT	η*	σ*
Ethyl acetate	10.53	369	1.511	14.17	507	1.550	19.92	707	1.435
Acetonitrile	5.08	389	1.612	5.02	374	2.097	8.74	622	1.768
Acetone	21.77	662	1.358	15.18	471	1.371	19.43	590	1.329
Methanol	22.54	879	1.145	21.26	853	1.384	21.36	871	1.257
Acetic acid	-	-	-	30.97	1841	1.370	29.32	1824	1.331

Figure 9a reveals the influence of the cooling rate in the four different solvents. It is expected [56] that the metastable zone width will increase with increasing cooling rate. This is apparent in acetonitrile and methanol but less clear in acetone, and in ethyl acetate the metastable limit appears to have reached its maximum at 10 °C/hr. The appearance of a plateau in metastable zone width with increasing cooling rate agrees with previous results on salicylamide[55].

18
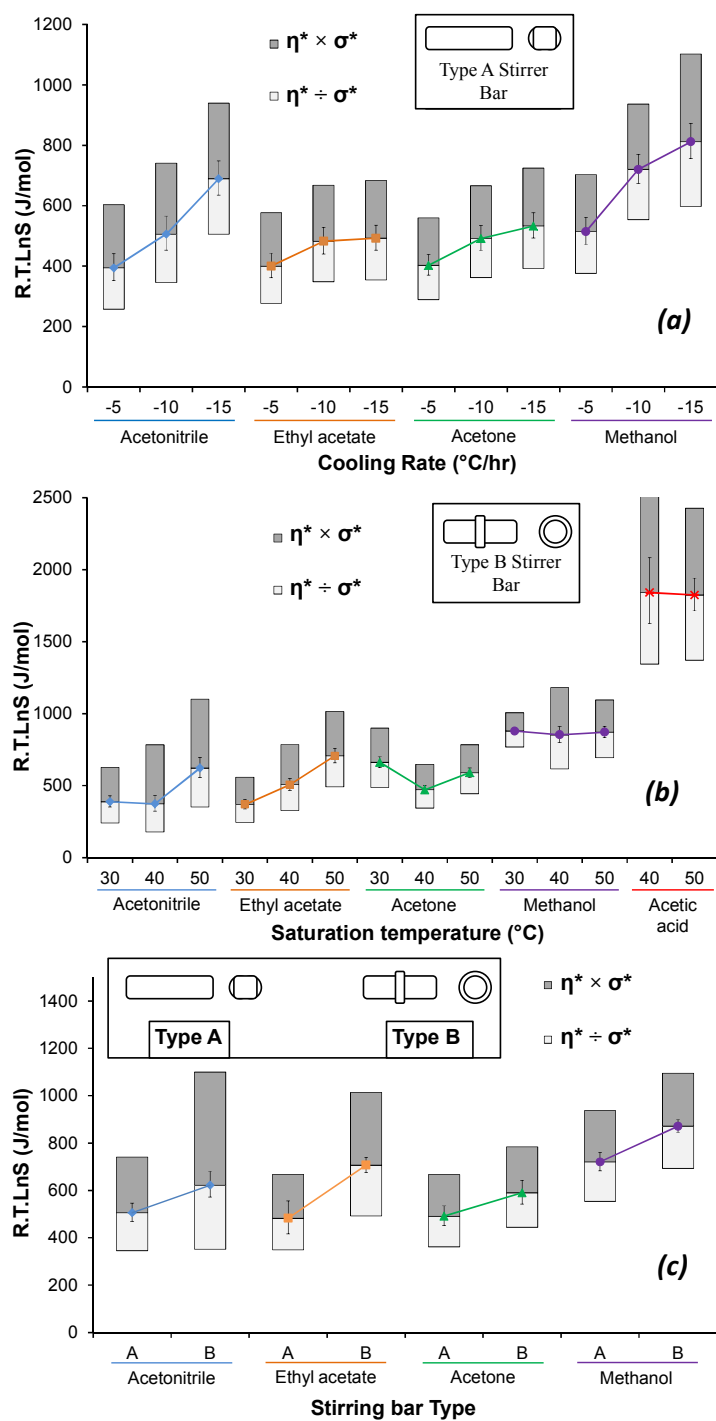
Figure 9. Influence of (a) solvent (b) saturation temperature and (c) stir bar type on the metastable zone width. Geometric mean (η^*) metastable zone widths with the error bars representing 95% confidence intervals for the geometric mean. The upper and lower shaded

regions bound one geometric standard deviation from the geometric mean ($\eta^* \times/ \sigma^*$) representing 68 % of the data. Saturation temperature: 50℃ for (a) and (c). Stir bar type as indicated on the diagram, 200 rpm.

The influence of the saturation temperature at constant cooling rate is presented in Figure 9b. Overall, there was no consistent correlation between the saturation temperature and the metastable zone width. The metastable zone width increases with increasing saturation temperature in ethyl acetate, the trend is somewhat the same in acetonitrile, while in methanol and acetic acid there is no impact at all. Due to the high freezing temperature of acetic acid (M.P = 16 ^{o}C) the cooling range was limited in this solvent. At saturation temperature 50°C, less than 70% of the acetic acid vials nucleated within the viable range, and at saturation temperature 40°C less than 25%. Accordingly no experiments at 30°C saturation temperature were performed, and for the same reason acetic acid was not included in the investigation of the influence of the cooling rate.

Figure 9c compares the results at 50 °C saturation temperature and 10 °C/hr cooling rate for the two different stir bars. The metastable zone width on average is consistently wider for experiments using the type B stir bar, which although shorter than the type A stir bar does contain a pivot ring. It is proposed that during rotation, the presence of the pivot ring holds the bulk of the stir bar above the bottom of the vial, resulting in lower shear rates, resulting in a lower rate of nucleation[57].

The experimental data clearly reveals that the widest metastable zone width for nucleation of salicylic acid is found in acetic acid (Figure 8). In acetic acid solutions saturated at 50 or 40 °C a large proportion of the vials didn't nucleate. Among the rest of the solvents, the methanol system reached higher RTlnS values and greater undercooling before nucleation occurred at all cooling rates for solutions saturated at 50 °C (Table 4), and at all saturation concentrations at 10 C/hr cooling rate (Table 5), Among the remaining three solvents there is no clear order.

DISCUSSION

Figure 10 compares the principles of the induction time and metastable zone width methods with respect to their temperature vs time profiles. Induction time experiments (IDT) establish a sudden step change in temperature and measure the time taken for nucleation to occur. Metastable zone width (MSZW) experiments employ a constant cooling rate to bring about nucleation and measure the temperature at which nucleation occurs.
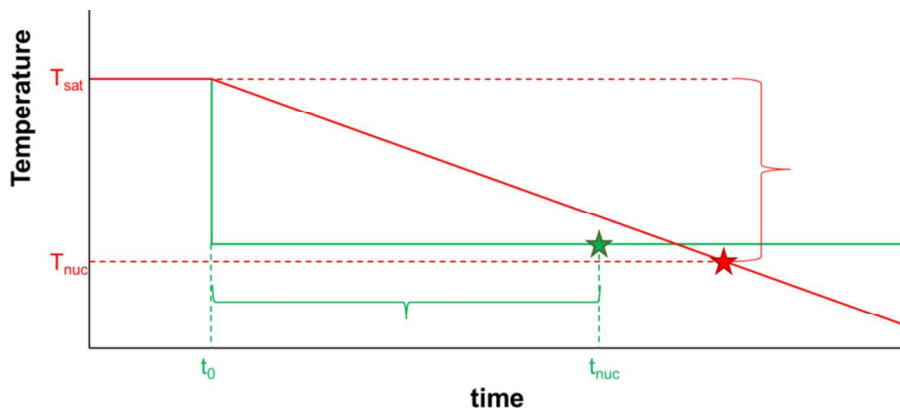
Figure 10. Measurement principals of induction time ($t_{ind} = t_{nuc} − t_0$) and metastable zone width ($\Delta T = T_{sat} − T_{nuc}$) techniques. Nucleation points are represented by green (induction time) and red (metastable zone width) stars.

It is not surprising that the order between the solvents in the MSZW experiments is not in full agreement with the order in the IDT experiments. In the MSZW experiments the average rate of nucleation will increase with time because of the increasing supersaturation. However, associated with each level of supersaturation is an induction time of nucleation as determined in the induction time experiments. In interpreting the MSZW experiments, it is necessary to consider the impact of induction time in these results.

At equal cooling rate, the rate of supersaturation generation in the solvents differs as a result of differences in the slope of the solubility curves. In Figure 11, the MSZW experiments are plotted as driving force versus temperature of each nucleation event for solutions saturated at 50 °C. At constant and equal cooling rate in the different solvents the temperature at which nucleation is observed corresponds directly to the time of nucleation. In terms of decreasing temperature/increasing time, on average (the black points) the nucleation appears first in acetonitrile followed by ethyl acetate, acetone and finally in methanol. However, in terms of increasing supersaturation driving force as reported above, the nucleation on average appears first in ethyl acetate followed by acetone, acetonitrile and methanol. On average, nucleation in acetonitrile occurs at a high RTlnS after the shortest period of time. A clearly lower median driving force is required in acetone but the time is also much longer. Obviously, to interpret MSZW experiments in relation to IDT experiments, account must be given to the supersaturation driving force at nucleation as well as the time for which the solution has been supersaturated.
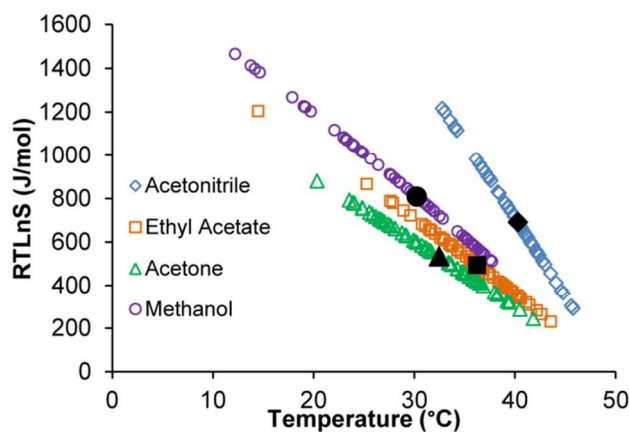
Figure 11. Nucleation in MSZW experiments. Data points represent nucleation events of salicylic acid from solutions saturated at 50 °C, cooled at 15 °C/hr. The geometric mean of each data set is also shown as a black dot.

In Figure 12, induction time results are compared with the metastable zone width data for acetonitrile. The x-axis represents the driving force at nucleation and the y-axis the nucleation time. For the IDT experiments the driving force is given by the temperature to which the solution is cooled as quickly as possible, and the nucleation time equals the induction time. All individual experiments fall on a vertical line for each set-up of experimental conditions. The orange points represent the geometric mean induction times, and the solid orange curve represents the correlation between mean induction time vs RTlnS. In the MSZW experiments, the nucleation events appear on an almost straight line (dashed) of increasing driving force for each cooling rate. The nucleation time is the time to form a nucleus in the solution of gradually increasing supersaturation and decreasing temperature. The black points represent the geometric mean (η*) driving force and the corresponding time of nucleation for the three different cooling rates. In Figure 13, the corresponding presentation is made for the other three solvents but only including geometric mean induction time and geometric mean metastable zone width values, and the accompanying 95% confidence intervals. The length of the dashed line cooling curves represents the range of experimental metastable zone width determinations.

Figure 11 very clearly illustrates the randomness of the nucleation at each condition. At the same conditions, respectively, IDT experiments can nucleate very early as well as very late, and MSZW experiments can nucleate at very low driving force as well as at high. At the point where the MSZW experiment line (dashed) intersects with the solid orange IDT curve, the time of nucleation is equal in the two types of experiment. If nucleation occurs at this point in the MSZW experiments, the induction time required to form nuclei is fully incorporated into the

time of cooling. Since at each level of supersaturation there is an induction time required for nuclei to form, it is not expected that the median time of nucleation in the MSZW experiments would be lower than this intersection point. Hence, the time of this intersection represents a minimum time for nucleation in the MSZW experiments. As shown in Figure 12, in acetonitrile, the average MSZW nucleation at all cooling rates occurs after this intersection, suggesting that the kinetic events behind the induction time (responsible for transforming clusters into stable nuclei) are not fast enough to be negligible compared to the rate of cooling. Thus the MSZW nucleation will lag behind the corresponding IDT nucleation. It is noteworthy though that the individual MSZW nucleation data points spread very widely on both sides of these intersection points. Similarly, in ethyl acetate (Figure 13a) the geometric mean MSZW nucleation occurs clearly after the intersection with the solid orange IDT curve. In acetone (Figure 13b) and methanol (Figure 13c), the overall behavior is the same but the lag is clearly less. In acetone and methanol the time lag initially increase with increasing cooling rate but then tends to decrease somewhat after a maximum. For acetonitrile and ethyl acetate the time lag, at least initially, decreases at increasing cooling rate. At 15°C/hr there is still a distinct time lag but the difference between the solvents is within about 800 s. This behavior does not correlate with the slope of the respective solubility curve.
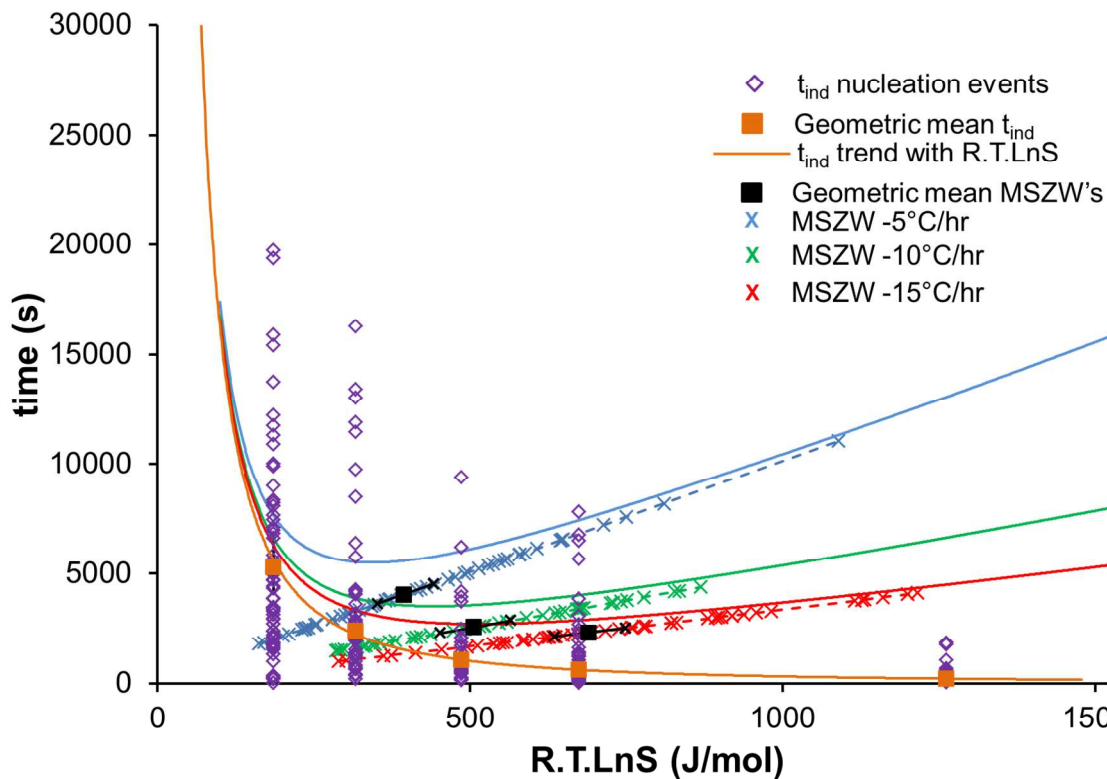
Figure 12. Comparison of induction time and metastable zone width experiments in acetonitrile. Induction time data (◊), geometric mean induction times (■), metastable zone width data; 5 °C/hr (**X**), 10 °C/hr (**X**) 15 °C/hr (**X**), and geometric mean metastable zone widths (■) of salicylic acid in acetonitrile. Solid orange line correlates the median induction time data. Solid blue, green and red lines represents the sum of the solid orange line (median induction time) and the dashed line (cooling time: blue 5 °C/hr, green 10 °C/hr, and red 15 °C/hr) at each driving force.
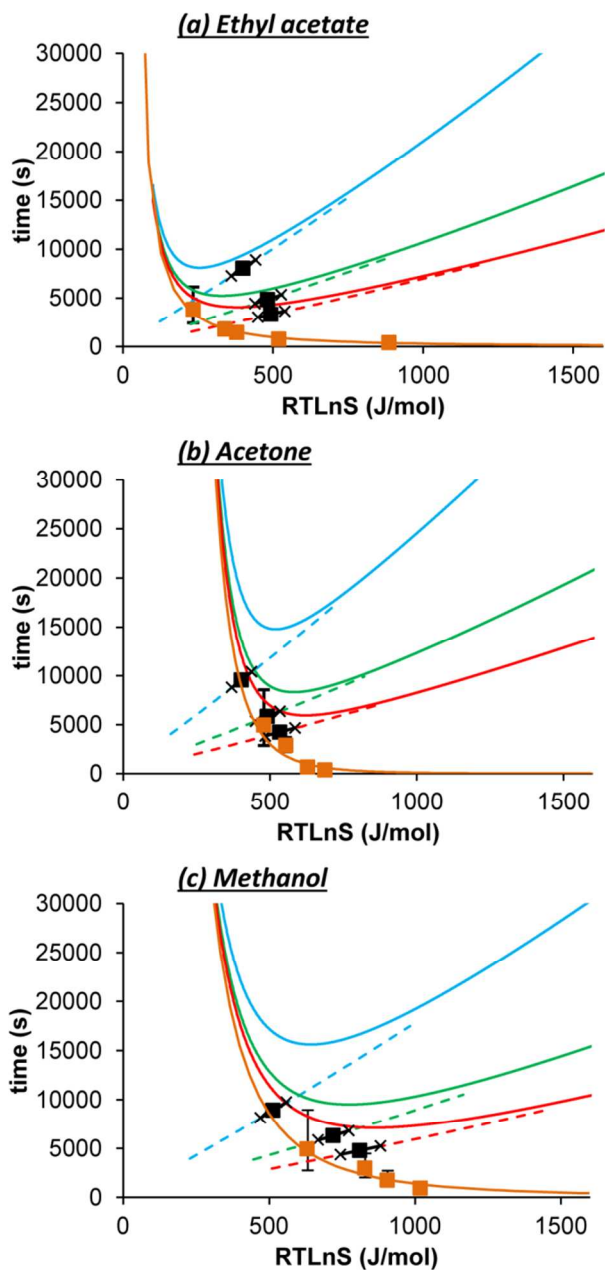
Figure 13. Comparison of induction time and metastable zone width experiments Geometric mean induction times (■), and metastable zone widths (■). Error bars represent 95% confidence intervals for the mean. Solid orange line correlates the median induction time data. Solid blue, green and red lines represents the sum of the solid orange line (median induction time) and the dashed line (cooling rate: blue 5 °C/hr, green 10 °C/hr, and red 15 °C/hr) at each driving force.

In Figures 12 and 13, each concave solid line matching a dashed cooling line of the same colour represents the sum of the IDT curve and the dashed MSZW cooling time curve at each driving force. These concave lines accordingly represent the situation where the solution is first cooled down at a constant rate to a certain driving force, and then is allowed to nucleate as if the supersaturation had been reached by a temperature change equal to that in the induction time experiments. This curve represents <u>a maximum time of nucleation in the metastable zone width experiments</u>. Experimentally we find that the nucleation in the MSZW experiments always occurs below this concave curve, revealing that the molecular reorganization behind forming a nucleus can proceed at least partly in parallel to the gradual increase in supersaturation. In acetonitrile and ethyl acetate, the mean MSZW nucleation time is in the order of 10^3 s below the corresponding maximum time. In methanol and acetone this value is much larger especially at low cooling rate. In all solvents, this time difference as expected decreases with increasing cooling rate, however much more so in acetone and methanol.

A relative MSZW nucleation time can be defined using the definitions of the minimum and maximum nucleation times stated above as the (MSZW Geometric Mean – Minimum Nucleation Time) / (Maximum Nucleation Time – Minimum Nucleation Time). In Figure 14a, the relative MSZW nucleation time, as defined above, is plotted as a function of cooling rate for each solvent. The graph clearly shows that in ethyl acetate and acetonitrile the metastable zone width nucleation occurs closer to the "maximum nucleation time", while in acetone and methanol the nucleation occurs closer to the "minimum nucleation time" especially at low cooling rate. Of course, the lag in the MSZW nucleation can be resolved into a time lag (difference in time between the geometric mean MSZW nucleation and the orange IDT curve) and a corresponding "*driving force rise*". Figure 14b shows that in ethyl acetate and acetonitrile, the driving force rise is larger than in acetone and methanol, and especially so at the lowest cooling rate. It is also shown that the driving force rise in acetonitrile, methanol and acetone systematically increases with increasing cooling rate as is expected, while in ethyl acetate there is no clear change. Accordingly, in acetone and methanol, the driving force rise at low cooling rate is much lower and the time lag is clearly lower than in acetonitrile and ethyl acetate. This behavior does not correlate with the slope of the respective solubility curves.

26
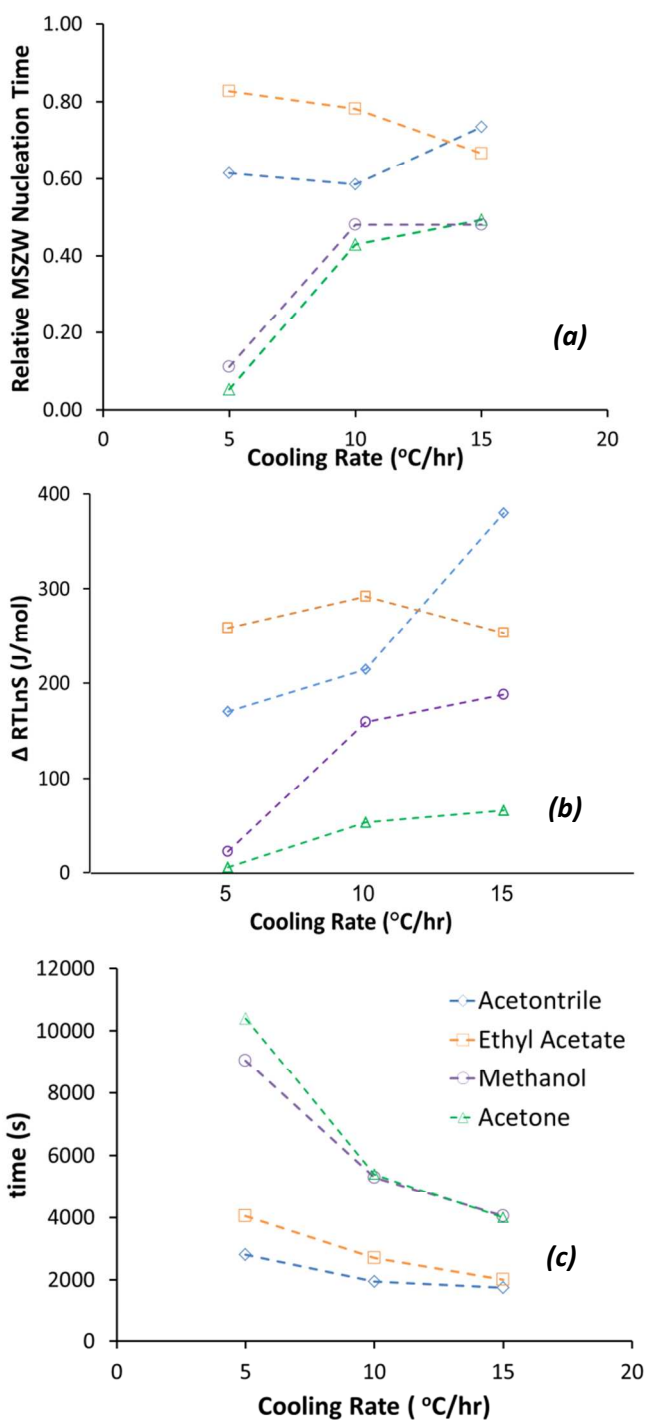
Figure 14. (a) Relative MSZW nucleation time, (b) "Driving force rate" and (c) Time of the intersection between the MSZW experimental line and the geometric mean of the induction time

data (solid orange line in previous graphs) in the same solvent, as a function of cooling rate in all solvents.

It is at first surprising that the MSZW nucleation lags behind the IDT nucleation more in acetonitrile and ethyl acetate, where according to the induction time experiments the nucleation at equal driving force is faster. However, for ethyl acetate and acetonitrile the induction times at comparable driving force are lower than in acetone and methanol. Thus the time of intersection between the MSZW experiment line and the solid orange IDT curve is shorter. As is shown in Figure 14c, for acetonitrile the intersection times are the lowest followed by those of ethyl acetate, and for acetone and methanol these values are approximately 1.5 - 3 times higher. Accordingly at the point of intersection in the MSZW experiments in the acetone and methanol solutions, more time has been allowed for the molecular level rearrangements that are required for nuclei to appear. This clearly points to the importance of the induction time component of the nucleation in the MSZW experiments.

The governing equation of the classical nucleation theory, Eq 7, contains a pre-exponential factor describing the rate by which molecules are attaching to a nucleus of critical size, which depends on the rate of molecular transport in the solution and the size of the nuclei. The equation further contains an exponential term, in which the nucleation work, Eq 8, describes the free energy barrier that needs to be surpassed for a cluster to turn into a nucleus. The nucleation work increases with increasing interfacial energy and decreasing supersaturation driving force. Even though the pathway of formation of a nucleus is different, the recently developed two-step model, also contains kinetic and thermodynamic components of the nucleation process. Molecular clustering can occur in the solution regardless of supersaturation, and the clusters may be distributed in size as well as in structure. Clusters are molecular assemblies that are thermodynamically unstable at the prevailing conditions, either because of insufficient size (classical nucleation theory) and/or, insufficient ordering/crystallinity (two-step nucleation theory). The steady-state cluster distribution is governed essentially by solute concentration and temperature, besides of course being dependent on the molecular properties of the solute and the solvent. Within the classical nucleation theory the increasing supersaturation in the metastable zone width experiments, reduces the nucleation work, ΔG_{crit} (Eq. 8) required to form a nucleus, thus leading to a reduction of the critical nucleous size (Eq. 10). However, nuclei don't form immediately in a supersaturated solution, and time is required to allow for the transformations to take place necessary to form thermodynamically stable crystalline nuclei. As revealed by the induction time curve, this time to nucleate decreases with increasing supersaturation. However, the analysis suggests that the required molecular level transformations are slow enough compared to the cooling rate, to influence the results of the MSZW experiments. Obviously, the interpretation of metastable zone width experiments is more complex than that of the induction

time experiments, but the combination of these data provides new valuable insights into nucleation phenomena.

CONCLUSIONS

The nucleation of salicylic acid in all six solvents revealed wide induction time distributions within the approximately 50 experiments performed at each condition. Metastable zone width distributions displayed the same degree of randomness at all cooling rates and solution concentrations examined. The log-normal distribution function is found to provide the best representation of these distributions, but the effect of using different cumulative distribution functions to reduce the nucleation data for determination of interfacial energies within the framework of the classical nucleation theory was found to be minimal. The results reveal that nucleation is influenced by the detailed shape of the magnetic stir bar. The solvent is found to have a strong influence on the nucleation of salicylic acid. Overall, the experimental results suggest that the induction time at equal driving force increases in the order: chloroform, ethyl acetate, acetonitrile, acetone, methanol, and acetic acid. The very same order is found for increasing interfacial energies as determined within the framework of the classical nucleation theory. In the metastable zone width experiments, it is found that acetic acid solutions have the widest metastable zone width followed by methanol solutions, after which there is no clear order between the remaining solvents. In examining the experimental outcome of the metastable zone width experiments against the corresponding induction time results, it is concluded that the outcome of the former is influenced by the rate by which supersaturation is generated as well as the rate of the moleculartransformations turning clusters into nuclei. Besides the time of cooling there is an additional time component by which metastable zone width nucleation lags behind induction time nucleation.

ACKNOWLEDGEMENTS

SYMBOLS

A	Kinetic factor of nucleation
C	Concentration
τ_{50}	Median
ΔG	Free energy of nucleation
J	Nucleation rate
k	Boltzmann's constant
M	Molecular mass
N_a	Avogadro's number
R	Gas constant
S	Supersaturation
t_{ind}	Induction time
T	Temperature
ΔT	Metastable zone in terms of temperature
υ	Molecular volume in critical cluster
V	Volume
x	solubility (mole fraction)

η	Mean of the lognormal distribution
η^*	Geometric mean
μ	Chemical potential
ρ	Crystal density
σ	Standard deviation of the lognormal distribution
σ^*	Geometric standard deviation
φ	Interfacial energy

Subscripts:

crit	Critical
eq	Equilibrium
nuc	Nucleation
sat	Saturation

REFERENCES

1.   J. W. Gibbs, On the equilibrium of heterogeneous substances / by J. Willard Gibbs, The Academy, New Haven, 1874.

2.   R. Becker and W. Döring, Annalen der Physik, 1935, **416**, 719-752.

3.   M. Volmer, Kinetik der Phasenbildung, Steinkopff Edwards, Ann Arbor, Mich., 1939.

4.   J. B. Zeldovich, ACTA PHYSICOCHIMICA URSS, 1943, **18**, 1-22.

5.   P. G. Vekilov, Cryst Growth Des, 2010, **10**, 5007-5019.

6.   J. Chen, B. Sarma, J. M. B. Evans and A. S. Myerson, Crystal Growth & Design, 2011, **11**, 887-895.

7.   W. Pan, A. B. Kolomeisky and P. G. Vekilov, The Journal of chemical physics, 2005, **122**, 174905.

8.   D. Erdemir, A. Y. Lee and A. S. Myerson, Acc Chem Res, 2009, **42**, 621-629.

9. Davey, R. J.; Schroeder, S. L. M.; ter Horst, J. H.,. Angewandte Chemie International Edition**, 2013,** 52, (8), 2166-2179.

10.   J. P. Leonard and J. S. Im, Applied Physics Letters, 2001, **78**, 3454-3456.

11.   H. Kakinuma, Jpn J Appl Phys 1, 2003, **42**, 3545-3548.

12.   O. Pino-García and Å. C. Rasmuson, Industrial & Engineering Chemistry Research, 2003, **42**, 4899-4909.

13.   D. Knezic, J. Zaccaro and A. S. Myerson, J Phys Chem B, 2004, **108**, 10672-10677.

14.   M. Svärd, F. L. Nordström, T. Jasnobulka and Å. C. Rasmuson, Crystal Growth & Design, 2010, **10**, 195-204.

15.   L. Goh, K. Chen, V. Bhamidi, G. He, N. C. Kee, P. J. Kenis, C. F. Zukoski, 3rd and R. D. Braatz, Cryst Growth Des, 2010, **10**, 2515-2521.

16.   S. Jiang and J. H. ter Horst, Crystal Growth & Design, 2011, **11**, 256-261.

17.   K. Chen, L. Goh, G. He, P. J. A. Kenis, C. F. Zukoski and R. D. Braatz, Chemical Engineering Science, 2012, **77**, 235-241.

18.   M. Svärd, F. L. Nordström, E.-M. Hoffmann, B. Aziz and Å. C. Rasmuson, CrystEngComm, 2013, **15**, 5020.

19. Kadam, S. S.; Kramer, H. J. M.; ter Horst, J. H., Crystal Growth & Design, **2011,** 11, (4), 1271-1277.

20.   P. Laval, A. Crombez and J. B. Salmon, Langmuir : the ACS journal of surfaces and colloids, 2009, **25**, 1836-1841.

21.   T. W. Barlow and A. D. J. Haymet, Review of Scientific Instruments, 1995, **66**, 2996-3007.

22.   Y. Diao, A. S. Myerson, T. A. Hatton and B. L. Trout, Langmuir : the ACS journal of surfaces and colloids, 2011, **27**, 5324-5334.

23.   W. Cochran, Acta Crystallographica Section E Structure Reports Online, 1953, **6**, 260-268.

24.   F. L. Nordstrom and A. C. Rasmuson, J Chem Eng Data, 2006, **51**, 1668-1671.

25.   A. Shalmashi and A. Eliassi, Journal of Chemical & Engineering Data, 2008, **53**, 199-200.

26.   H. Matsuda, K. Kaburagi, S. Matsumoto, K. Kurihara, K. Tochigi and K. Tomono, Journal of Chemical & Engineering Data, 2009, **54**, 480-484.

27.   R. A. Granberg, C. Ducreux, S. Gracin and A. C. Rasmuson, Chemical Engineering Science, 2001, **56**, 2305-2313.

28.   S. Teychené and B. Biscans, Crystal Growth & Design, 2008, **8**, 1133-1139.

29.   M. Svärd and Å. C. Rasmuson, Crystal Growth & Design, 2013, **13**, 1140-1152.

30.   M. C. Etter, Accounts of Chemical Research, 1990, **23**, 120-126.

31.   S. Janbon, R. J. Davey and G. Dent, The Journal of Physical Chemistry C, 2008, **112**, 15771-15776.

32.   M. Janik, Z. Malarski, J. Mroziński, J. Wajcht and Z. Zborucki, Journal of Crystallographic and Spectroscopic Research, 1991, **21**, 519-522.

33   R. J. Davey, N. Blagden, S. Righini, H. Alison, M. J. Quayle and S. Fuller, Crystal Growth & Design, 2000, **1**, 59-65.

34.   R. J. Davey, N. Blagden, S. Righini, H. Alison and E. S. Ferrari, The Journal of Physical Chemistry B, 2002, **106**, 1954-1959.

35.   W. I. Cross, N. Blagden, R. J. Davey, R. G. Pritchard, M. A. Neumann, R. J. Roberts and R. C. Rowe, Crystal Growth & Design, 2002, **3**, 151-158.

36.   S. Gracin and A. C. Rasmuson, Crystal Growth & Design, 2004, **4**, 1013-1023.

37.   V. M. Profir and Å. C. Rasmuson, Crystal Growth & Design, 2004, **4**, 315-323.

38.   R. A. Chiarella, A. L. Gillon, R. C. Burton, R. J. Davey, G. Sadiq, A. Auffret, M. Cioffi and C. A. Hunter, Faraday discussions, 2007, **136**, 179-193; discussion 213-129.

39.   R. J. Davey, G. Dent, R. K. Mughal and S. Parveen, Crystal Growth & Design, 2006, **6**, 1788-1796.

40.   D. Kashchiev and G. M. van Rosmalen, Crystal Research and Technology, 2003, **38**, 555-574.

41.   K. P. Liang, G. White, D. Wilkinson, L. J. Ford, K. J. Roberts and W. M. L. Wood, Industrial & Engineering Chemistry Research, 2004, **43**, 1227-1234.

42.   N. P. Rajesh, C. K. L. Perumal, P. S. Raghavan and P. Ramasamy, Crystal Research and Technology, 2001, **36**, 55-63.

43   K. J. Kim, M. J. Kim, J. M. Lee, S. H. Kim, H. S. Kim and B. S. Park, J Chem Eng Data, 1998, **43**, 65-68.

44. Kulkarni, S. A.; Kadam, S. S.; Meekes, H.; Stankiewicz, A. I.; ter Horst, J. H., Crystal Growth & Design **2013,** 13, (6), 2435-2440.

45. Sullivan, R. A.; Davey, R. J.; Sadiq, G.; Dent, G.; Back, K. R.; ter Horst, J. H.; Toroz, D.; Hammond, R. B., Crystal Growth & Design, **2014,** 14, (5), 2689-2696.

46.   E. Limpert, W. A. Stahel and M. Abbt, BioScience, 2001, **51**, 341-352.

47.   D. G. Bonett, Computational Statistics & Data Analysis, 2006, **50**, 2953-2957.

48.   J. W. Mullin and S. Zacek, Journal of Crystal Growth, 1981, **53**, 515-518.

49.   P. H. McMurry, M. Fink, H. Sakurai, M. R. Stolzenburg, R. L. Mauldin, J. Smith, F. Eisele, K. Moore, S. Sjostedt, D. Tanner, L. G. Huey, J. B. Nowak, E. Edgerton and D. Voisin, Journal of Geophysical Research: Atmospheres, 2005, **110**, D22S02.

50.   R. Zhang, L. Wang, A. F. Khalizov, J. Zhao, J. Zheng, R. L. McGraw and L. T. Molina, Proceedings of the National Academy of Sciences of the United States of America, 2009, **106**, 17650-17654.

51.   R. Zhang, Science, 2010, **328**, 1366-1367.

52.   Y. Diao, K. E. Whaley, M. E. Helgeson, M. A. Woldeyes, P. S. Doyle, A. S. Myerson, T. A. Hatton and B. L. Trout, J Am Chem Soc, 2012, **134**, 673-684.

53.   W. Omar, M. Mohnicke and J. Ulrich, Crystal Research and Technology, 2006, **41**, 337-343.

54.   C. M. Hansen, in Hansen Solubility Parameters, CRC Press, 1999.

55   F. Nordström, M. Svärd, and, Å.C. Rasmuson, Crystal Engineering Communications, 2013, 15 (36), 7285 – 7297

56.   J. Nývlt, R. Rychlý, J. Gottfried and J. Wurzelová, Journal of Crystal Growth, 1970, **6**, 151-162.

57.   J. Liu and Å. C. Rasmuson, Crystal Growth & Design, 2013, **13**, 4385-4394.

58.   Huaiyu Yang, Michael Svärd and Åke C. Rasmuson; *Crystal Growth & Design, 14* (8), 3890–3902, 2014